Rapid phenol mineralisation in a low-pressure dead-end light transmitting photocatalytic membrane reactor (LT-PMR)

Journal of Water Process Engineering 66 (2024) 106018

Contents lists available at ScienceDirect

Journal of Water Process Engineering

journal homepage: www.elsevier.com/locate/jwpe

Rapid phenol mineralisation in a low-pressure dead-end light transmitting photocatalytic membrane reactor (LT-PMR)

Peter Sanciolo [a], Kana Moriguchi [b], Noel Dow [a], Fotios Sidiroglou [a], Tomohisa Yoshioka [c], Keizo Nakagawa [c], Mikel Duke [a,*]

[a] Institute for Sustainable Industries & Liveable Cities, Victoria University, 70-104 Ballarat Road, Footscray 3011, Australia
[b] Department of Chemical Science and Engineering, Kobe University, 1-1 Rokkodai, Nada, Kobe 657-8501, Japan
[c] Research Center for Membrane and Film Technology, Graduate School of Science, Technology, and Innovation, Kobe University, 1-1 Rokkodai, Nada, Kobe 657-8501, Japan

ARTICLE INFO

Editor: Ludovic F. Dumée

Keywords:
Photocatalysis
Membrane reactor
Microfiltration
Titania
Phenol
Mineralisation

ABSTRACT

Photocatalytic membrane reactors (PMRs) are widely studied for wastewater decontamination but reactions are too slow for scaled up application. This PMR study proposes a novel operation involving rapid decontamination in just one pass through the confined space within the membrane. This approach was demonstrated for the first time by light transmitting PMR (LT-PMR), conveniently receiving UV LED light (λ_{peak} = 365 nm) via the permeate side to the photocatalyst P25 TiO_2 microfiltration membrane coated on porous glass. A 93 % reduction in model contaminant phenol concentration from a 10 mg/L feed occurred at a flux of 4.7 L/m^2/h. The phenol degradation occurred without any additional residence time from external vessels or recirculation. Phenol was almost entirely mineralised, confirmed by total organic carbon (TOC) measurements, with trace by-products identified by high pressure liquid chromatography (HPLC) analysis. Mass transfer and reaction rate constants from Langmuir-Hinshelwood modelling were comparable to literature. Highest reaction rates occurred at lowest permeate phenol concentrations, highlighting potential to destroy recalcitrant pollutants persisting through established treatments. LT-PMR is therefore an effective and practical process that very rapidly destroys phenol. Further work to explore improved flux by enhanced light transmission, tailored catalytic materials and demonstration on other pollutants and water matrices is warranted.

1. Introduction

There is a growing need for water treatment systems to allow communities world-wide to utilise sources of water such as industrial waste and stormwater to improve water security and reduce demand on natural resources. Reuse of these potential water resources is limited due to the known presence of many trace organic contaminants (TrOCs) such as toxic industrial chemicals that are typically not removed by existing treatment systems [1]. Advanced treatments to remove these contaminants include "dense" membrane filtration by low pressure reverse osmosis (LPRO) membranes. These processes can remove many organic contaminants, but not all of these contaminants are easily rejected, especially those of lower molecular weight. Furthermore, the LPRO process concentrates salt components along with the rejected TrOCs in its waste brine stream, exacerbating an already significant disposal issue [2]. Alternatively, non-residual forming treatments such as advanced oxidation processes (AOPs) employ powerful hydroxyl radicals that can eliminate TrOCs by mineralising them to predominantly innocuous products including water, carbon dioxide and mineral acids. Scale up of AOPs, however, remains a challenge [3]. Yet one promising commercially scalable AOP is photocatalysis.

Photocatalysis for water treatment, driven by artificial UV light or sunlight, has been studied for many years for water remediation application, particularly using TiO_2 based photocatalysts [4]. The rising concerns of the health and environmental impact of contaminants and the growing availability of renewable energy and low cost UV LEDs has sparked renewed research interest in this technology. Many research studies deal with the degradation of model compounds, and a particularly good candidate with respect of toxicity and prevalence is phenol. Tests using the well-studied commercial TiO_2 P25 photocatalyst [5,6] in batch reactors have shown that the phenol in a 12 mg/L solution requires 2 h to degrade by >90 %, and 8 h to mineralise (reduced total organic carbon concentration) by the same extent [7]. To improve

* Corresponding author.
E-mail address: mikel.duke@vu.edu.au (M. Duke).

https://doi.org/10.1016/j.jwpe.2024.106018
Received 29 April 2024; Received in revised form 29 July 2024; Accepted 16 August 2024
Available online 31 August 2024

Nomenclature

A_{mem}	membrane effective area (m^2)
a_i	interfacial area per unit volume of liquid phase in the photocatalytic layer (m^2/m^3).
α	exponent representing influence of UV irradiance (−)
β	light absorption coefficient (1/m)
C_0	concentration at $z = 0$ (mol/m^3)
C_F	Feed concentration (mol/m^3)
C_L	concentration (mol/m^3) at catalyst bed thickness $z = L$
C_P	Permeate concentration (mol/m^3)
$C_{S(z)}$	concentration at the membrane surface at location z (mol/m^3)
$C_{(z)}$	bulk solution concentration of the reactant species at location z (mol/m^3)
ε	porosity of the immobilised coating (m^3 pore/m^3 total volume)
$I_{0,1}$	light intensity reaching the catalyst surface first test (W/m^2)
$I_{0,2}$	light intensity reaching the catalyst surface second test (W/m^2)
I_L	measured light leaving the membrane coating on the feed side (W/m^2)
J	membrane flux ($L/m^2/h$)
K_{ad}	adsorption equilibrium constant (m^3/mol)
$K_{i,0}$	combined reaction rate constant of the top layer of the catalyst bed (1/s)
K_{res}	overall reaction rate constant of the catalyst layer (1/s)
k_m	mass transfer coefficient (m/s)
k_{res}	intrinsic reaction rate constant per unit cross-sectional area of the catalyst layer (m/s)
$k(z)$	reaction rate constant at location z ($mol/(m^3.s)$)
L	catalyst bed thickness (m)
m_P	mass permeate collected over test sampling interval (kg)
m_{Ptot}	total permeate mass collected (kg)
m_R	mass of the collected purged reject (kg)
R	reduction of phenol (wt%)
$r(z)$	intrinsic reaction rate at location z ($mol/(m^3/s)$)
ρ_{cat}	density of the catalyst particle (kg/m^3)
ρ_P	permeate solution density at test conditions (= 1.0 kg/L)
S_{cat}	specific surface area of catalyst particle (m^2/kg)
t_{int}	test interval time (h)
V_F	superficial velocity (m/s)
VR	volume recovery (vol%)
z	distance from location where light first contacts the catalyst coating

reactivity, researchers have explored numerous materials and their modifications. One example considered TiO_2 modifications with graphitised carbon composites which showed a >6-fold increase in photocatalytic activity towards phenolic compounds compared to the reference commercial P25 TiO_2 photocatalyst [4].

As a means to address practical challenges of physically separating photocatalysts from the treated water, researchers have studied its combination with membrane filtration as a photocatalytic membrane reactor (PMR) for TrOC removal [8], which also has the benefit for maintaining the membrane itself by reducing membrane fouling [9–11]. One specific type of PMR involves immobilised photocatalysts, creating a unique benefits to not only achieve the original photocatalytic degradation of the target pollutants and size selective separation of the membrane, but also eliminate the problematic separation of the mobile photocatalyst [12]. A study involving immobilisation of P25 on steel plates showed 44 % phenol degradation after 3 h of photocatalysis in synthetic air [13]. An important motivation of this study was to also assess the more rarely reported (but practically more important) extent of mineralisation as measured by total organic carbon (TOC) assays. Measurement of the TOC before and after treatment in this literature study revealed that only <10 % TOC reduction had been achieved, indicating incomplete phenol mineralisation. Schwarze et al. 2023 found that another photocatalyst, P90, together with dosing hydrogen peroxide gave a more favourable 70 % reduction in TOC in the 3-h test period.

All these prior tests showed the treatment potential of immobilised PMRs, but required crossflow or recirculating dead-end systems and treatment times in the order of hours for meaningful pollutant reduction [8,11,14], necessitating the use of large tanks and high energy pumps when scaled up, leading to high capital and running costs. Further, some of these PMR studies also feature contaminant molecule retention, which may lead to the same byproduct formation issues mentioned above for LPRO if the contaminant is still not destroyed. A recent development has been the operation of immobilised PMR in dead-end mode to react and destroy small organic pollutant molecules passing *once through* the membrane. This promises to be a significant practical improvement where the contaminants undergo the catalysed degradation reactions as they are forced through the porous photocatalyst coating [15,16]. This has the potential to enhance the extent and rate of reactions by maximising contact of the contaminants with the photocatalyst. This potential was highlighted with P25 coated on porous alumina which showed reduction of up to 21 % of model toxic pollutant phenol at 6 mg/L through the membrane at 34.5 $L/m^2/h$ flux with the light directed to the feed side [17].

Another recent development is treatment by a novel light transmitting PMR (LT-PMR) process [18–20]. In LT-PMR the light is transmitted to the photocatalytic coating from *underneath* (i.e. via the clear permeate to the interface between the substrate and catalyst), thus avoiding all the challenges associated light blockage by turbid feed water and accumulated foulants. The LT-PMR concept easily integrates into existing high packing density monolith designs commonly used in full scale water treatment plants using ceramic membranes by simply utilising a transparent material as a substrate, like glass, and directing light, e.g. sunlight, from the outside-facing permeate side [21]. The new LT-PMR featuring P25 dip-coated on porous glass substrate uniquely allowed light to be distributed into the photocatalyst in counter-current to flux. These works demonstrated significant reduction in membrane fouling using UV light generated by a LED [19] and simulated sunlight [18], and highlighted the potential for significant improvements to membrane fouling resistance using photoactive materials also being discovered by others [22]. The fluxes in the prior LT-PMR studies were, however, too high (up to 450 $L/m^2/h$) for contaminant destruction through the membranes.

The current study aims to improve overall degradation using LT-PMR, maximising contact of contaminant and photocatalyst and minimising energy requirement by operating at lower flux (5 $L/m^2/h$ to 12 $L/m^2/h$) and in dead end mode, i.e., without any recirculation of permeate back to the feed. The results are analysed using modelling of reaction and mass transfer as previously employed for recirculating dead-end tests [16] to relate to prior studies and to understand reaction kinetics and mass transfer in the current study. The modelling required two light intensity tests to derive the relevant reaction and mass transfer constants. The P25 material was utilised again as the TiO_2 coating due to its wide availability and the abundance of published photocatalysis results, enabling discussions to compare to performance of the novel LT-PMR concept. This is the first known work exploring the contaminant destruction potential in the significantly simplified *once through* process approach by LT-PMR that addresses light access challenges identified in

current literature state of the art PMR designs. The goal is to progress LT-PMR as a practically viable technology for sustainable water reuse.

2. Experimental

2.1. Materials

All chemicals were analytical grade and used as received. NaCl (99.9 % Ajax Finechem, Scoresby, Australia) and phenol (≥99 % Sigma Aldrich, St. Louis, MO, USA) were used to prepare the model contaminant test solutions. Titanium dioxide P25 nanoparticles with 99.8 % purity with 80 % anatase and 20 % rutile phases, average particle size of 30 nm, and a specific surface area of 50 m^2/g (Degussa AG, Frankfurt, Germany). Sintered glass discs used as the light transmitting porous glass substrates (PGS) had a 25 mm diameter, 2 mm thickness and G5 porosity with pore size of 1.5 μm [19], sourced from Ningbo Ja-Hely Technology Co., Ltd., Ningbo, China.

2.2. Membrane fabrication

The membranes were prepared by dip coating one side of PGSs with a suspension of Degussa P25 TiO_2 in water and sodium alginate, followed by air drying and sintering as described in detail in previously reported work [19]. The method involved mixing 5 g TiO_2 powder with 60 mL water and 0.4 g sodium alginate to act as a binder, followed by high-speed homogenisation and sonication to remove lumps and air bubbles. The PGSs were then mechanically dipped into the suspension with one side masked by tape, followed by air drying for 12 h and heating in a muffle furnace to 450 °C at a rate of 1 °C/min. Controlled cooling at a slow rate was employed to prevent cracking, followed by washing in DI water and drying at 80 °C for 2 h. Our prior studies on LT-PMR using membranes fabricated by the same method were analysed by surface and cross section SEM to have an intact P25 coating with 15 μm thickness, consisting of nano-sized particles. The mean pore size measured by porosimetry was 0.53 μm, classifying it as a microfiltration membrane. The surface structure exhibited no observable changes after repeated UV light exposure and was tested with model fouling materials, humic acid, sodium alginate and bovine serum albumin [18,19]. Visual inspection and optical microscopy were used to select two of the fabricated membranes with the most intact surface appearance for testing in the LT-PMR. Their samples codes were L1 and L2.

2.3. Filtration setup and testing

The membrane filtration equipment used in this study is depicted diagrammatically in Fig. 1. The membrane was placed between two O-rings in a custom-made stainless steel filtration module, to give an effective membrane area A_{mem} of 0.00031 +/− 10 % m^2. A 1.2 W, 365 nm ultraviolet light emitting diode (UV-LED) (MTE3650L2-UV-HP, DigiKey Electronics, Minnesota, USA) was mounted directly under a quartz window located underneath the module, allowing light to transmit through the permeate side of the membrane disc located 12.6 mm from the quartz window as previously reported [19]. The LED had a narrow emission bandwidth (supplier specified spectral line half width @ 100 mA = 15 nm), with the maximum power output occurring at the wavelength of 365 nm. It featured a pulsed signal to avoid overheating (total pulse period = 2.04 ms. 15 % on, then 85 % off) was controlled using an Arduino control board, operating at 2.2v with a current of 260 mA. For reduced light intensity testing, the UV light was attenuated using Mylar A film of 0.125 mm thickness (RS-Components, type 785–0798) as a filter and placed directly on the quartz window inside the module. The potential for UV degradation of the filter, thereby altering its transmission, was controlled by ensuring transmitting light intensity at the end of the test was within 10 % of the initial (new installed film) reading. The UV intensity emitted by the LED at 365 nm was measured by a UV irradiance meter (Photoelectric Instrument Factory of Beijing Normal University, Beijing) placed directly on the open module with no openings for light to escape at a distance of 22 mm from the internal permeate window.

Membrane testing was conducted in constant flux mode to best represent full scale microfiltration plants in water treatment. The feed was accurately supplied to the membrane according to the flux set point by a NE-1000 single syringe pump (New Era, USA), which is a positive displacement type pump that uses a constant speed motor drive to deliver constant flow into the test module. The feed pressure during filtration was recorded using a TPI 665 L digital manometer (Accutherm, Melbourne, Australia), although no pressure was detected during all testing (<1 kPa). An electronic balance (FX-3000i WP, A&D Company Ltd., Seoul, South Korea) with real time monitoring software was used to measure the amount of permeate (membrane filtrate) produced during the experiments, allowing calculation of actual membrane flux, J ($L/m^2/h$) according to Eq. 1:

$$J = \frac{m_P}{\rho_P A_{mem}\, t_{int}} \tag{1}$$

where m_P (kg) is the mass of permeate over the measurement interval time, t_{int} (h), and ρ_P is the permeate solution density assumed = 1.0 kg/L for the relatively dilute solutions at room temperature conditions. The measured flux error of +/− 5.5 % was calculated from the precision of the balance and estimation of membrane area. As testing was conducted in dead-end mode, the reject was purged after a long test period to remove any accumulate rejected material mimicking full scale microfiltration plants which often operate at permeate volume recovery, *VR*,

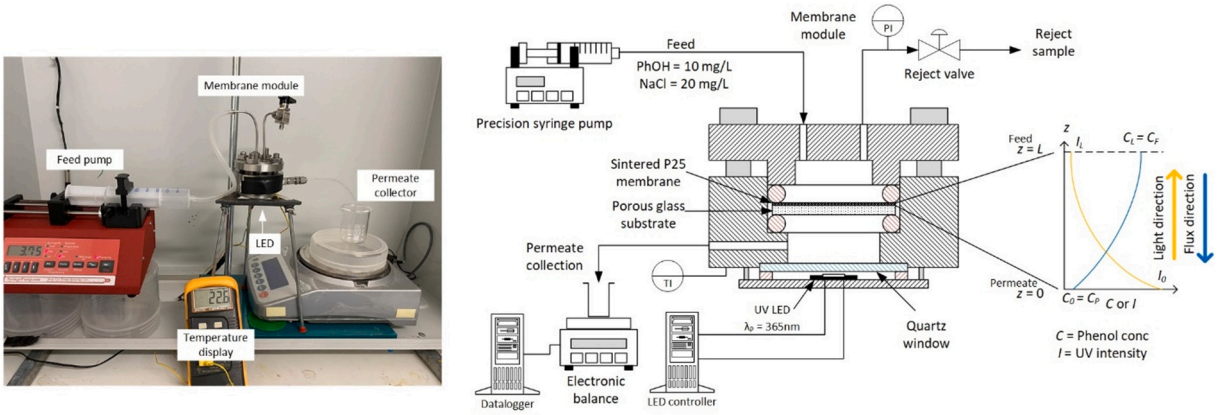

Fig. 1. Image of experimental setup (left) and schematic diagram (right) showing the working concept of the counter-current LT-PMR where light transmission through the photocatalyst coating occurs is in the opposite direction to the flux of the feed solution. TI = temperature indicator, and PI = pressure indicator.

exceeding 90 %. For these experiments, *VR* was calculated according to Eq. 2:

$$VR = \frac{m_{Ptot}}{m_{Ptot} + m_R} \quad (2)$$

where m_{Ptot} is the total permeate mass collected in the operating cycle, m_R is the mass of the collected purged reject (kg). The assumption in Eq. 2 is that both m_{Ptot} and m_R solutions have the same density allowing volume recovery to be directly calculated by their measured weights.

All tests were carried out with a model contaminant feed solution made with 10 mg/L phenol in 20 mg/L NaCl mixed into DI water. The choice of phenol concentration represents typical residual phenol concentrations from treatments of much higher phenol concentration feeds by other treatment methods [23], that are still regarded as toxic to humans and aquatic life. The NaCl concentration was chosen simply as a background electrolyte that has an important presence representing real water matrices as used in our prior LT-PMR studies [19]. PGS and membranes were immersed in test solution overnight prior to commencing filtration to minimise start-up instabilities due to phenol adsorption on to the PGS and P25 coating. As the UV LED emits heat into the membrane module, temperature was monitored using a thermocouple and maintained at 25 °C, +/− 2 °C by gentle heating with a 40 W halogen lamp directed at the outside of the module when the UV LED was not in use (i.e. dark testing).

The membrane photocatalysis experiment plan consisted of five key tests, where the imposed conditions in each step within a test are summarised in Table 1. Tests 1 to 3 were designated for confirmation of photocatalytic degradation involving PGS, L1 and L2 respectively as a means to ensure comparable results between two identically made and visibly intact membranes (L1 and L2) against the uncoated PGS substrate. Test 4 was designated for extended photocatalysis performance on L1 to explore numerous steps representing flux set points of 5.0, 7.5 and 12 L/m^2/h together with light off/on step changes. Test 5 featured attenuated light testing at the same fluxes on L1. Testing at any prescribed condition was considered to be sufficient once steady state in the permeate phenol concentration was measured, and values averaged from the last 2–3 stable fluxes, feed and permeate concentrations. These average values were used for model input.

Table 1
Summary of the test sequence and conditions implemented during all tests on L1, L2 and PGS. UV light was unattenuated unless indicated as attenuated using the Mylar A filter by "att."

Test number	Test step	Membrane	UV LED status	Flux setting (L/m^2/h)	Purpose
1	A	PGS	Off	5.0	Stable condition used for model. HPLC sample collected
	B	PGS	On	5.0	Stable condition used for model. HPLC sample collected
2	A	L1	Off	5.0	Stable condition used for model. HPLC sample collected
	B	L1	On	5.0	Stable condition used for model. HPLC sample collected
3	A	L2	Off	5.0	Stable condition used for model. HPLC sample collected
	B	L2	On	5.0	Stable condition used for model. HPLC sample collected
4	A	L1	Off	7.5	Initial stabilisation
	B	L1	On	7.5	Stable condition used for model. TOC sample collected
	C	L1	On	12	Stable condition used for model.
	D	L1	Off	12	Stable condition used for model.
	E	L1	Off	7.5	Stable condition used for model. TOC sample collected
	F	L1	On	5.0	Stable condition used for model.
	G	L1	Off	5.0	Stable condition used for model. Test ended
5	A	L1	On (att.)	5.0	Attenuated light test. Stable condition used for model.
	B	L1	On (att.)	7.5	Attenuated light test. Stable condition used for model.
	C	L1	On (att.)	12	Attenuated light test. Stable condition used for model.

2.4. Sample characterisation

A UV–visible light spectrophotometer (HACH DR5000, USA) was used to measure phenol concentration in the samples in a 1 cm quartz cell. Four calibration standards were made ranging from 1 mg/L to 10 mg/L to cover the full range of expected test concentrations. A preliminary scan of the solution found a peak light absorbance $\lambda_{max} = 270$ nm, and was used to prepare the calibration curve from the standards ($r^2 > 0.999$) and analyse all feed and permeate samples. Calibrations were re-done prior to each testing period. An error of +/− 0.13 mg/L in the phenol measurements was calculated from replicate spectrophotometric measurements of the feed concentration during the experiments. Reduction, *R*, of phenol was calculated from permeate and feed concentrations (C_P and C_F respectively) and presented as a percentage according to Eq. 3:

$$R = \left(1 - \frac{C_P}{C_F}\right)100 \quad (3)$$

The TOC of test solutions was determined by thermal oxidation with NIR detection from a Shimadzu TOC-V CSH analyser (Shimadzu Corporation, Kyoto, Japan). The concentration of phenol contaminants was analysed by Shimadzu Nexera XR high performance liquid chromatography (HPLC) system (Shimadzu Corporation, Kyoto, Japan). The instrument is equipped with an auto sampler (SIL-40C XR), a system controller (SCL-40), solvent delivery pump (LC-40B XR), degassing unit (DCU-403), column oven (CTO—40S) and an Ultraviolet-Visible (UV–Vis) detector (SPD-40). A TSKgel ODS-120H (19 μm, 2.0 × 50 mm) column was used for chromatographic separations. The mobile phase consisted of 5:95 HPLC-grade acetonitrile (ACN) (≥99.9 % Fujifilm Wako Pure Chemical Corporation, Osaka, Japan): ultrapure water mixed with 0.1 vol% HPLC-grade formic acid (≥99.5 % Fujifilm Wako Pure Chemical Corporation) at a flow rate of 0.3 mL/min. The column temperature was maintained at 30 °C and the injection volume was 5.0 μL. The sample run time was 10 min. ACN used as extracting solvent was filled in a 2 mL HPLC vial and treated as solvent blank. The UV–vis detector was set at 270 nm for acquiring chromatograms. Phenol (≥99 %), *p*-benzoquinone (≥98 %), hydroquinone (≥99 %) (Fujifilm Wako Pure Chemical Corporation) and catechol (≥99.5 %, Sigma Aldrich) were used to prepare calibration solutions. The calibration solutions at concentrations of 0, 2.5, 5.0, 7.5, 10.0, and 12.5 mg/L were prepared and calibration curves were prepared for each substance.

2.5. Reaction modelling

Reaction modelling to determine reaction rate and mass transfer constants was guided by prior studies on PMRs. Early modelling work on PMRs considered first order kinetics at the low concentrations typically present in water remediation (e.g. ~10 mg/L) on membranes and over

coated films [24]. Further development of the model included mass transfer in recirculating dead-end filtration mode where the photocatalyst was loaded onto the membrane surface immediately prior to contaminant degradation [16]. The model accounts for the steps of 1 – diffusion of reactants from bulk to the catalyst surface, 2 – adsorption of the reactant on to the photocatalyst surface, 3 – photocatalytic reaction of the reactants, 4 – desorption of reacted by-products and 5 – diffusion of reacted by-products into the bulk solution. The model was applied to determine reaction rate constants that account for the light intensity variation while diffusing through a catalyst bed loaded on to the membrane surface. The diffusion and adsorption steps 1 and 2 were considered to be much faster than the reaction step 3, and therefore the intrinsic reaction rate at any location z through the catalyst bed, $r(z)$, (mol/(m^3/s)) can be represented by the Langmuir-Hinshelwood model as described by Eq. 4:

$$r(z) = -\frac{\partial C_{(z)}}{\partial t} = \frac{k(z)K_{ad}C_{S(z)}}{1 + K_{ad}C_{S(z)}} \tag{4}$$

where $C_{(z)}$ is the bulk solution concentration of the reactant species (mol/m^3), $C_{S(z)}$ is the concentration at the membrane surface (mol/m^3), $k(z)$ is the reaction rate constant (mol/(m^3.s)), at location z (m), and K_{ad} is the adsorption equilibrium constant (m^3/mol). The reaction rate was assumed to equal the diffusion rate representing steady state step 1 as described by Eq. 5:

$$r(z) = k_m a_i \left(C_{(z)} - C_{S(z)}\right) \tag{5}$$

where k_m is the mass transfer coefficient (m/s) and a_i is the interfacial area per unit volume of liquid phase in the photocatalytic layer (m^2/m^3). Including functions to account for reaction rate decline with decreasing light penetration into the photocatalyst bed, and assuming plug flow within the bed, the change in concentration that occurs on permeation through the catalyst bed in the fixed bed PMR was described by Eq. 6:

$$ln\frac{C_L}{C_0} = -\frac{k_m a_i}{\alpha\beta L} ln\frac{k_m a_i + K_{i,0}}{k_m a_i + K_{i,0}e^{-\alpha\beta L}} t_{res} = -K_{res}t_{res} \tag{6}$$

where C_L is the concentration (mol/m^3) at catalyst bed thickness L (m) in the direction of flow (equivalent to the permeate concentration in this arrangement), C_0 is the concentration (mol/m^3) at $z = 0$ (equivalent to feed concentration in this example), α is the exponent representing influence of UV irradiance (−), β is the light absorption coefficient (1/m), $K_{i,0}$ is the combined reaction rate constant of the top layer of the catalyst bed (1/s), and K_{res} (1/s) is the overall reaction rate constant of the catalyst layer. Eq. 6 was applied to experimental data to determine mass transfer (k_m) and reaction rate ($K_{i,0}$) parameters to analyse PMR performance, where at least two light intensity experiments were needed to solve as simultaneous eqs. [16]. For further analysis, the parameter k_{res} (m/s) was proposed representing the intrinsic reaction rate constant per unit cross-sectional area of the catalyst layer as described by Eq. 7:

$$k_{res} = K_{res}L \tag{7}$$

However, since Eq. 6 was originally derived for co-current light transmission with flux direction, The LT-PMR system in the present study works in counter-current (light enters from the permeate side) as shown in Fig. 1. The relevant counter-current model is therefore achieved by maintaining the location of light entrance at $z = 0$, but swapping the concentration positions so that $C_0 = C_P$ (permeate concentration) and $C_L = C_F$ (feed concentration), and reversing the sign of the function to accommodate for $C_{(z)}$ to increase in the direction of light transmission (as considered in the original relationship form of Eq. 4), represented for convenience in terms of feed and permeate concentrations for the LT-PMR in the present study as described by Eq. 8:

$$ln\frac{C_F}{C_P} = \frac{k_m a_i}{\alpha\beta L} ln\frac{k_m a_i + K_{i,0}}{k_m a_i + K_{i,0}e^{-\alpha\beta L}} t_{res} = K_{res}t_{res} \tag{8}$$

To obtain K_{res} from experimental data, the permeate concentration, C_P, for a given flux, J (L/m^2/h) needs to be presented according to residence time, t_{res} (s) as described by Eq. 9:

$$t_{res} = \frac{L\varepsilon}{V_F} = \frac{L\varepsilon}{J} \times 3600000 \tag{9}$$

where ε is porosity of the immobilised P25 coating, which has been taken as 0.34 m^3 pore/m^3 total from prior studies on immobilised P25 coatings [25], and V_F is the superficial velocity (m/s). Normally K_{res} would be calculated from experimental data by Eq. 8 using a graph of ln (C_F/C_P) vs t_{res}, and obtaining the slope of the linear fit, allowing calculation of k_{res} by Eq. 7. However, in the prior fixed bed PMR modelling [16] it was found that k_{res} varied considerably with flux (superficial velocity) due to the changes in mass transfer associated with changed flow through the bed. Instead, K_{res} was calculated by simply dividing ln (C_F/C_P) by t_{res} for every stabilised constant flux test (at least three fluxes tested) to allow evaluation of k_{res} change with t_{res} as a result of changing mass transfer conditions. The mass transfer coefficient k_m that appears in Eq. 6, which the same researchers assumed is identical while testing two light intensity tests at identical fluxes, was calculated using Eq. 10:

$$\frac{I_{0,1}}{I_{0,2}} = \frac{exp\left(\frac{\beta k_{res,1}}{k_m a_i}\right) - 1}{exp\left(\frac{\beta k_{res,2}}{k_m a_i}\right) - 1} \tag{10}$$

where $I_{0,1}$ and $I_{0,2}$ are the light intensities reaching the catalyst surface (W/m^2) for the first and second light intensity tests, respectively. β is the light absorption coefficient (1/m) calculated experimentally according to Eq. 11:

$$\beta = \frac{1}{L} ln\frac{I_0}{I_L} \tag{11}$$

where I_L is the measured light leaving the membrane coating on the feed side (W/m^2), which is easy to conduct in the LT-PMR as this is the accessible feed side of the membrane that is exposed when the membrane module is open. The determined k_{res} values, as described above from Eq. 7 for the two light intensity tests, was entered into Eq. 10, leaving the lumped constant $k_m.a_i$ to be readily solved by computer iteration, which represents the total mass transfer coefficient in the LT-PMR at each tested flux.

Interestingly, the combined reaction rate constant of the top layer of the catalyst bed $K_{i,0}$ as also shown in Eq. 8 assuming the simplification following a limiting case of $\frac{K_{i,0}}{k_m a_i}e^{-\alpha\beta L} << 1$ which can also be calculated using Eq. 12 [16]:

$$K_{i,0} = k_m a_i \left(exp\left(\frac{k_{res}\alpha\beta}{k_m a_i}\right) - 1\right) \tag{12}$$

This equation relies on the value the exponent representing influence of UV irradiance (α), where previously $\alpha = 1$ has been used on the condition that the $I_0 < 250$ W/m^2 [16]. Eqs. 8 to 12 provide the sufficient theoretical means and experimental direction to calculate the valuable parameters representing the overall reaction and mass transfer effects, allowing comparison of the LT-PMR in the current study to that in the literature for other immobilised photocatalyst reactors.

3. Results and discussion

3.1. Confirmation of light transmission to catalyst coating

The intensities of UV light (365 nm) were measured by the sensor located 21.6 mm above the quartz window (see Fig. 1), at various stages of solution filling and membrane installation are shown in Fig. 2. The sensor was fully enclosed by the module compartment, preventing entry of light from outside or escape of LED light. With only the phenol feed

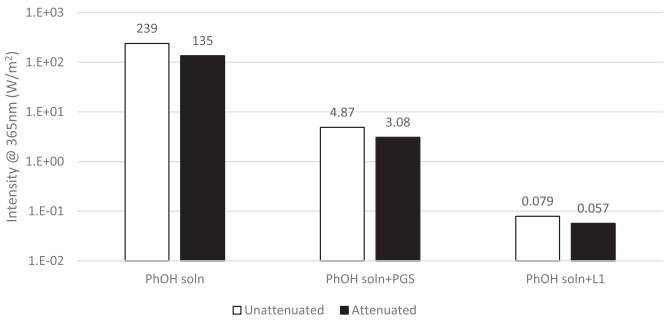

Fig. 2. Intensities of UV light measured at wavelength of 365 nm at various solution fill and membrane installation stages in the PMR module, including with installed Mylar-A filter installed for attenuated light intensity tests. PGS is the uncoated porous glass substrate, while L1 is the same PGS plus P25 photocatalyst coating. UV sensor was located on opening of PMR module at a distance of 21.6 mm from the quartz window with UV LED (λ_{peak} = 365 nm) mounted immediately below.

solution in the module, the light intensity was 239 W/m^2 which was reduced to 135 W/m^2 in the presence of the Mylar A filter. When the porous glass substrate (PGS) was added to the module, the light intensity dropped significantly to around 2 % of the original value, being 4.87 W/m^2 without the filter (unattenuated), and 3.08 W/m^2 with the filter installed (attenuated). This light energy is considered to be equivalent to what would be incident to the catalyst coating, i.e. I_0. There is clearly a substantial proportion of lost UV light within the PGS, which was not an optimised material for this application (glass filters sourced typically used in laboratory filtration). Improvement to the transmitted light through the PGS to the photocatalyst can be the focus of a separate study where we have reported potential polymer and inorganic candidates by other researchers investigating porous glass films in other applications [21]. With membrane L1 installed, consisting of a P25 coating on a PGS, a small level of UV was detected, with >98 % of the incident light to the photocatalyst (I_0) being absorbed within the P25 coating. The data was used to calculate extinction coefficient β using Eq. 11 as 265,976 1/m, which is lower than previously reported sintered P25 films with 34 % porosity at 626,400 1/m [25], while 144,300 1/m was assumed for pseudo-immobilised P25 (loaded in-situ) with at higher porosity of 84.9 % [16]. Our value is higher than the previously reported immobilised P25 film indicating more light extinction which may be due to the presence of phenol solution in the P25 coating (light intensity measured while soaked in feed solution), or that the coating in the current study was slightly more dense where linear correlation of porosity to extinction coefficient has been previously assumed where dense (0 % porosity) has a β of 949,100 1/m [26]. Therefore our measured value to calculate β appears valid for modelling the LT-PMR.

Another important point from this test was to confirm sufficient light energy for PMR operation for phenol degradation. Previous work with UV light applied directly to the titania photocatalyst utilised 100 W/m^2 [17] and from UV lamps with intensity as low as 15 W/m^2 [16]. Although higher than the current study values of UV light intensity to the photocatalyst as a result of attenuation through the PGS, they are valid for exploring the phenol degradation potential in the LT-PMR and the effect of the light intensity on reaction rate was analysed as part of the modelling.

3.2. Confirmation of photocatalytic degradation

The permeate phenol concentrations during constant flux testing at set flux of 5.0 L/m^2/h for both an uncoated PGS and identically made photocatalyst coated membranes L1 and L2 demonstrating LT-PMR (Tests 1–3) are shown in Fig. 3. The average of the measured phenol concentrations in the feed solutions for all three tests over the run duration was 10.1 mg/L (SD = 0.17 mg/L). Testing started in both cases with the LED off (dark) for at least 20 h. With the PGS alone, a gradual decline in concentration to 8.2 mg/L took place, with the last two data points averaging at 8.8 mg/L corresponding to phenol reduction of 12.9 %. The overall decline in concentration may be attributed to ongoing and slight phenol adsorption effects as a result of permeation. When the LED was switched on, the phenol concentration rose to 11 mg/L (exceeding feed concentration) and declined again, which may be due to some initial local heating effects releasing adsorbed phenol from P25 and/or PGS, followed by ongoing further adsorption. The average of the last two measured permeate phenol concentrations for the PGS test was 8.7 mg/L (14.2 % reduction) being very similar to the dark condition showing no significant reduction occurred due to photolysis within the PGS, and confirming the baseline value of approximately 14 % phenol reduction for PGS alone for use in the subsequent tests on photocatalyst coated membranes L1 and L2.

Starting first in dark conditions, photocatalyst coated membranes L1 and L2 showed reduction in phenol, stabilising with average permeate values at the end of the test period of 6.2 mg/L (38.9 % phenol reduction) for L1 and 7.8 mg/L (23.3 % phenol reduction) for L2 indicating some additional ongoing adsorption due to permeation as also seen on PGS. However as soon as the LED was switched on, both L1 and L2 behaved similarly and reduced phenol to an average of 1.5 mg/L (85.6 % phenol reduction) and 1.1 mg/L (89.4 % phenol reduction), respectively, in the last ~10 h of the test period. The observed reductions of

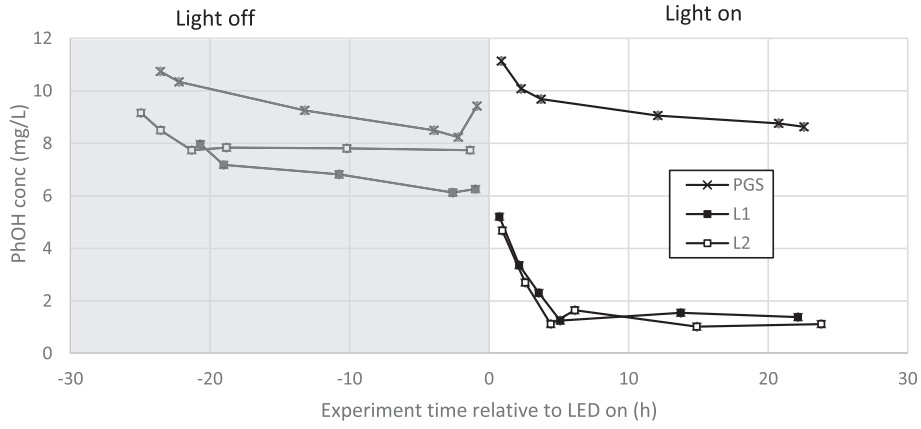

Fig. 3. Preliminary LT-PMR proof of operation test showing permeate phenol (PhOH) concentrations (error bars +/− 0.13 mg/L) relative to when the UV LED was switched on at flux set point of 5.0 L/m^2/h using uncoated porous glass substrate (PGS – Test 1) and P25 photocatalyst coated membrane reactor (LT-PMR) with two identically made membranes L1 (Test 2) and L2 (Test 3). Collected sample were used for HPLC analysis. I_0 = 4.87 W/m^2 (λ_{peak} = 365 nm). Feed: 10 mg/L phenol in 20 mg/L NaCl. Module temperature maintained at 25 °C, +/− 2 °C.

phenol without and with photocatalyst can be compared to prior work on 3-h batch tests showing negligible phenol degradation in UV without photocatalyst, but degraded by 56 % in UV light when 1 g/L photocatalyst was present [7]. In looking at a more relevant PMR system, previously reported work on conventional PMR (light facing the P25 photocatalyst) showed 21 % reduction of phenol through the membrane at a flux of 34.5 L/m^2/h [17]. In our work, the results shown in Fig. 3 confirmed that our experimental design to lower flux by ~7-fold compared to this prior PMR study, improved phenol reduction to ~90 %. The collected samples from each test step were reserved for HPLC analysis.

3.3. Extended photocatalysis performance

The results of the longer duration test, Test 4 as outlined in Table 1, are shown in Fig. 4. Starting initially with the UV-LED off (dark) at the intermediate flux setting of 7.5 L/m^2/h (Test 4A), the feed and permeate phenol concentrations were similar (10.0 mg/L +/− 0.6 mg/L) but had not stabilised before implementing the next test step. The UV-LED was first turned on after 1 h (Test 4B), which led to a drop in permeate phenol concentration stabilising after 5 h to an average of 2.9 mg/L (71.8 % phenol reduction). This condition remained stable over 22 h, where a sample was collected and reserved for TOC analysis. The flux set point was then increased to 12 L/m^2/h while the LED remained on (Test 4C), and permeate phenol concentration stabilised more rapidly to an average of 4.5 mg/L (54.6 % phenol reduction). This rise in permeate phenol concentration was expected as the residence time of phenol inside the PMR catalyst was reduced. Then at 26.8 h, the LED was switched off (Test 4D) and permeate phenol concentration rose as expected towards the feed concentration stabilising to an average of 9.0 mg/L (10.7 % phenol reduction). This phenol reduction is similar to that observed at 5.0 L/m^2/h presented in Fig. 3 and can be attributed to ongoing adsorption of phenol in the photocatalyst and PGS.

The flux setting was reduced again to 7.5 L/m^2/h while the PMR still operated in dark mode (Test 4E) and operated at this condition for another 13 h (to 46 h total operating time). Average stable phenol concentration was 8.3 mg/L (16.5 % phenol reduction). During the long stable operation, another TOC sample was collected from the permeate. In order to observe higher phenol reduction like the test in Fig. 3, from about 46 h the flux setting was dropped to 5.0 L/m^2/h, and shortly after the LED was switched on again (Test 4F). As expected, the permeate phenol concentration dropped significantly, reaching the average stable value of 0.71 mg/L (92.6 % phenol reduction). The flux setting of 5.0 L/m^2/h was maintained until 61 h total operation, where the LED was switched off (Test 4G) and as expected, permeate phenol started to rise. However as observed in the initial tests presented in Fig. 3, and the prior conditions in this test, it stabilised at a lower value than the feed, this time to an average of 7.3 mg/L (23.8 % phenol reduction).

In summary, this long test further demonstrated very high reductions of phenol (up to 92.6 %), where these reduction declined as expected as flux was increased. While most of this was due to photocatalysis, there is a smaller reduction in phenol through the membrane that cannot be attributed to photocatalytic reaction and was attributed to adsorption effects that persisted even after 20 h of testing. The experiments however provided accurate measurements of stabilised phenol concentrations at the three tested fluxes, at both UV on and off conditions, suitable data for input into the model. From a practical perspective, the flux setting of 5.0 L/m^2/h (measured average flux = 4.7 L/m^2/h) needed for the highest phenol reduction is on the lower end of industrial low pressure micro- and ultra-filtration plants, but more advanced catalysts with higher reactivity with improved reactivity photocatalysts such as 2D nanomaterials [27] could be used to achieve similar phenol degradation with at least 3-fold increase in flux levels. This is possible since the LT-PMR is a platform technology that can readily be integrated with such improved photocatalysts, as this work demonstrated the success of the concept for pollutant degradation using the widely used P25 as a reference.

3.4. LT-PMR phenol reduction performance summary

Fig. 5 summarises the measured values of permeate concentration at the average measured fluxes from Figs. 3 and 4 that were used for modelling (a), together with the corresponding reductions using the average of these permeate phenol concentrations (b). Additional data is presented for the attenuated light test I_0 of 3.08 W/m^2 (Test 5) needed for determination of the mass transfer and reaction parameters using Eq. 10. Close clustering of the measured phenol concentrations can be seen around the average values represented by the lines showing that the changes at each flux are significant. The reduced light showed similar permeate phenol concentration trend with flux, but as expected, consistently lower than the higher intensity (un-attenuated) test.

3.5. LT-PMR reject solution analysis

The ability of the membranes to reject the phenol was determined by sampling the feed solution in the module via the reject valve (see Fig. 1). The phenol concentration in samples taken at the light and dark periods are shown in Fig. 6. The volume recovery, *VR*, in these dead-end mode filtration experiments was 89 % (+/− 3 %) overall. A 10-fold increase in concentration in these samples would, therefore, be expected if phenol was rejected. This was not detected. Phenol rejection was not expected based on prior work on the same membranes applied for fouling

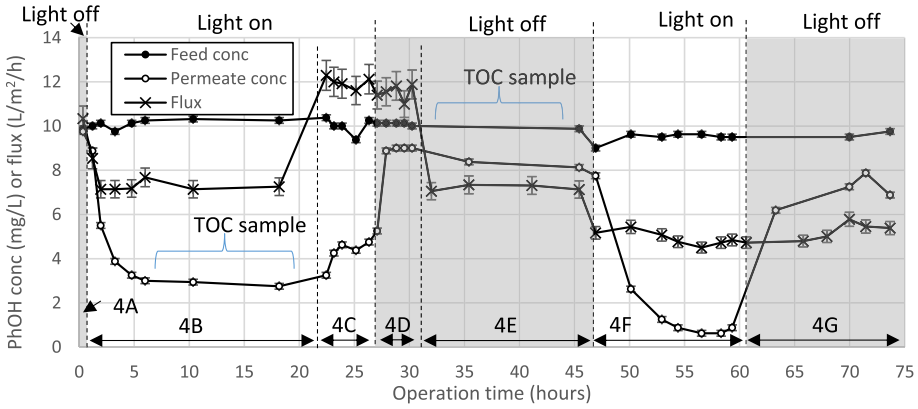

Fig. 4. Long test of LT-PMR membrane L1 following implemented flux settings and UV on/off conditions defined as Tests 4A to 4G in Table 1, showing measured feed and permeate concentrations measured by spectroscopy (error bars +/− 0.13 mg/L), and measured flux (error bars +/− 5.5 %). I_0 = 4.87 W/m^2 provided by UV LED (λ_{peak} = 365 nm). Extended testing periods to collect samples for TOC analysis as indicated. Module temperature maintained at 25 °C, +/− 2 °C.

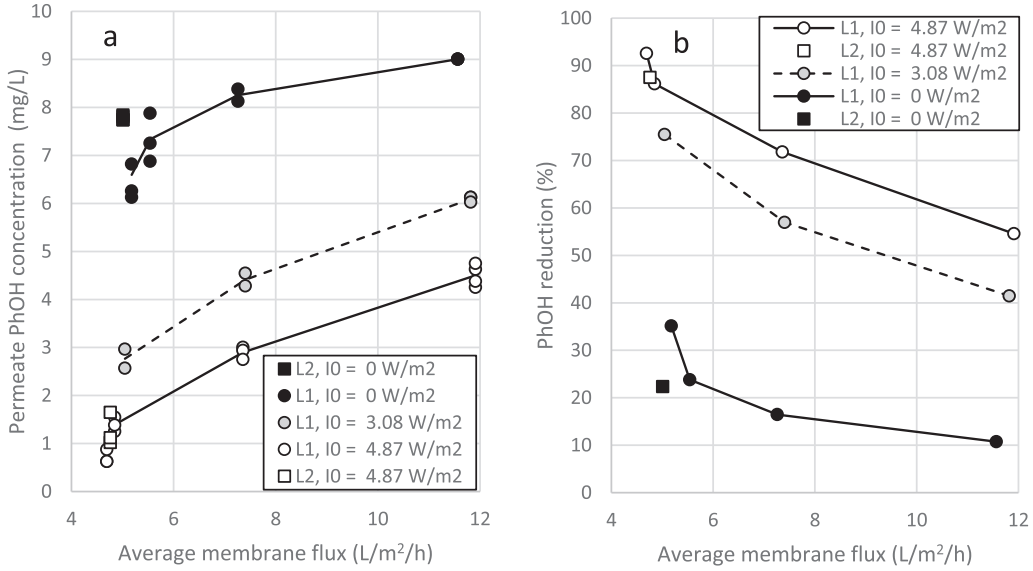

Fig. 5. Summarised spectroscopy measured values of permeate phenol concentrations at each flux period from all tests conducted on membranes L1 and L2 as presented in Figs. 3 and 4 presented with lines drawn between average values (a), and corresponding reductions determined by average of the phenol concentrations (b). Additional results from attenuated LT-PMR testing with L1 at I_0 of 3.08 W/m^2 (λ_{peak} = 365 nm) also included. Module temperature maintained at 25 °C, +/− 2 °C.

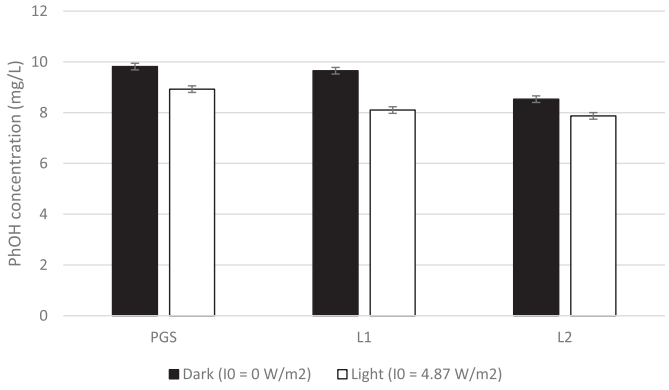

Fig. 6. Reject phenol concentrations (error bars +/− 0.13 mg/L) measured by spectroscopy for porous glass substrate (PGS) and duplicate P25 coated membranes L1 and L2 from tests presented in Fig. 3. Volume recovery at point of reject collection was measured at 89 % (+/− 3 %) across all tests.

reduction as the pore size is too large [18,19]. In all cases, consistently around 1–2 mg/L less phenol was measured in the reject when the light was on, even for the PGS which had no photocatalyst material. The degradation in all cases may instead be due to photolysis as the time until the reject collection was 15–20 h. In any case, it is interesting to note that the LT-PMR's ability to react with organic molecules by UV extends into the feed side, and can further degrade any caught material that is purged via the reject (including if performed by backwash).

3.6. Phenol degradation analysis by TOC and HPLC

The degree of phenol degradation by mineralisation was first determined using TOC measurements. Fig. 7 shows the TOC analysis results compared to phenol concentrations measured by spectroscopy, both in terms of mg-C/L (i.e., 1 mg/L of phenol = 0.766 mg-C/L) for the indicated TOC samples shown in Fig. 4 when testing at the flux set point of 7.5 L/m^2/h (measured average flux =7.4 L/m^2/h for light off, and 7.3 L/m^2/h for light on tests). Feed analysis results have been added for reference, and a slightly lower value of 1.2 mg-C/L was found for the spectroscopy assay compared to the TOC assay. In dark (light off) conditions, the feed TOC of 9.1 mg-C/L was reduced by 14 % while feed phenol of 7.9 mg-C/L was reduced by 19 % confirming earlier observations of adsorption occurring in dark conditions. When the UV light was applied (light on), these reductions increased to 63 % and 72 % respectively. Looking more closely at the carbon removed, TOC measured 9.1–3.4 = 5.7 mg-C/L where spectroscopy measured 7.9–2.2 = 5.7 mg-C/L which are very similar values thus giving strong evidence that essentially all phenol removed was by mineralisation. This level of mineralisation is considerably higher than previous batch mode studies on phenol degradation using P25 photocatalyst which only achieved <10 % TOC reduction and 70 % phenol reduction despite the much longer reaction times of 3 h [12]. This highlights a significant finding. The LT-PMR can be used for destruction of organics contaminants leaving no residuals in a relatively simple dead-end low pressure microfiltration membrane format. The phenol reduction and mineralisation took place in the brief time required for the liquid to pass only once through the membrane, thereby avoiding extended reaction vessel residence times that are problematic to scale up. Further analysis of the degradation by-products was conducted by HPLC.

The degradation pathways for phenol under UV irradiation has been previously investigated [28] and is shown in Fig. 8. Here we see that indeed mineralisation is possible where intermediates of catechol, hydroquinone, *o*-benzoquinone, *p*-benzoquinone and acetic acid could be measured if degradation was incomplete [6,28,29].

The phenol degradation was investigated using HPLC measuring catechol, benzoquinone and hydroquinone, from the samples presented in Fig. 3 and the results are shown in Fig. 9. The PGS showed some reduction in phenol compared to feed as evident in the spectroscopic assay data presented in Fig. 3, with no significant difference seen between permeate samples when the UV LED was on or off. Further, no degradation products were detected. For both L1 and L2 membranes, the light off test showed a further reduction in phenol compared to PGS, as also evident in the Fig. 3 data. When the LED was switched on, near complete elimination of phenol occurred for both membranes (reduced to 0.3–0.1 mg/L), while benzoquinone and hydroquinone by-products were found to be present in small concentrations (<1.1 mg/L) in both samples. Catechol was not detected, indicating either the likelihood of Pathway B presented in Fig. 8 for photocatalytic conversion of phenol to

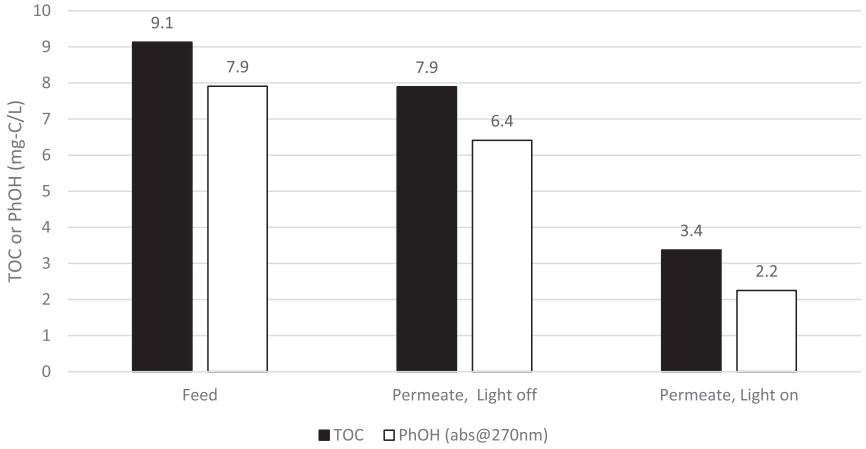

Fig. 7. TOC results analysis for samples collected as indicated in Fig. 4 while testing membrane L1. I_0 = 4.87 W/m^2 (λ_{peak} = 365 nm). Phenol concentrations measured by spectroscopy also shown, in TOC unified units of mg-C/L. Samples taken at measured average flux =7.4 L/m^2/h for light off, and 7.3 L/m^2/h for light on tests.

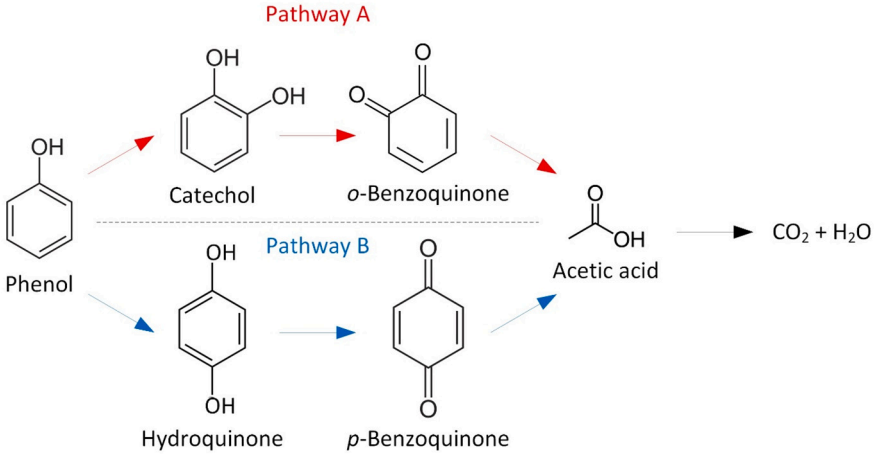

Fig. 8. Photocatalytic degradation pathways of phenol under UV irradiation from [28].

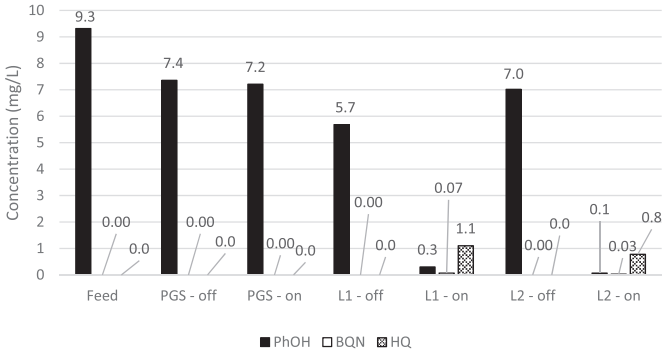

Fig. 9. HPLC results on feed, and various permeate samples (as indicated) showing identified species phenol (PhOH), benzoquinone (BQN) and hydroquinone (HQ). Catechol was not detected. Samples collected during Tests 1–3 (results shown in Fig. 3). I_0 = 4.87 W/m^2.

CO_2, and/or faster decomposition of catechol.

The photocatalytic oxidation of aromatic phenol has been related to its OH group, which is generally considered to be a strongly activating ortho and para directing substituent. This makes it highly prone to electrophilic substitution reactions. In prior mechanism studies on photocatalytic oxidation of phenol on illuminated TiO_2 powder in an air lift loop reactor, dihydroxybenzenes were the primary products due to the •OH attack on the phenol molecule. This was evident from tests after 3 h, with hydroquinone at the highest concentration in the products, followed by catechol then minor (detected but unmeasurable) proportions of resorcinol [30]. This aligns with the expected substitution reactions where •OH attack on the phenol molecule occurs more probably to the 2 and 4 positions, and uniquely hydroquinone accumulated due to its much lower reaction rate. This was also observed in Tao et al.'s later study in immobilised nano-ZnO [28], who also measured acetic acid as the additional product (aliphatic molecule) considered in mechanisms studies, leading to its inclusion in their proposed mechanism presented in Fig. 8. These prior studies on phenol therefore align with the current study findings where both benzoquinone and hydroquinone residuals were measured (with relatively more hydroquinone). Relatively minor amounts of these products were, however, detected in the permeate in the current study, indicating almost complete mineralisation of the phenol in the very brief time period required for the solution to permeate through the photocatalyst. This in contrast to the literature studies where mineralisation was incomplete despite operation times in the order of hours. These results are a demonstration of the practical improvement to the state of the art in PMR via the LT-PMR system targeting phenol with NaCl impurity, but can now be extended with future studies in the presence of other impurities, such as other electrolytes and natural organic matter (NOM) depending on the specific application [23]. Other target molecules instead of phenol can be

considered as well, for example well known TrOCs including herbicides, pesticides, polycyclic aromatic hydrocarbons, hormones and pharmaceuticals that persist in existing water treatment systems [1].

3.7. Reaction modelling

The results from all the tests across both membranes L1 and L2, in dark and the two light intensity conditions, are presented in terms of ln (C_F/C_P) for the calculated residence time, t_{res}, in Fig. 10a. The calculated k_{res} values as a function of superficial velocity (flux in units of m/s) are also shown in Fig. 10b. The graph of ln(C_F/C_P) vs residence time shows a linear correlation for most points at all conditions, except for the longest residence time of 3.91 s (or lowest flux of 4.7 L/m^2/h), where there was a sharp increase in the value correlating to a higher than expected reaction rate. The low phenol removal observed under dark conditions (I_0 = 0 W/m^2) (see Fig. 5), which was attributed to phenol adsorption and which resulted in no reaction by-products as observed by HPLC analysis, gave rise to a constant k_{res} of 1 × 10^{-6} m/s at superficial velocities above 1.5 m/s (most values). Despite numerous hours of steady operation, the phenol reduction remained constant for all tests and on both L1 and L2. In all cases, the graph of k_{res} vs superficial velocity (Fig. 10b) shows nearly flat responses (with the exception at lowest fluxes/highest residence times), indicating little influence on reaction from other factors such as mass transfer. The lack of a clear increase in k_{res} was surprising as intuitively higher flow through the catalyst coating would increase the reaction rate as observed in prior work [16]. The results are confirmed with the replicate membrane L2 test. Further analysis can be conducted using the calculated mass transfer and reaction rate constants from modelling.

Table 2 summarises the average measured flux, J, average superficial velocity, V_F, photocatalyst coating residence time, t_{res}, together with model fitted $\beta/k_m.a_i$ for each same flux condition using different light intensities (I_0), and total mass transfer coefficient $k_m.a_i$ calculated using Eqs. 8 to 12. During fitting, only flux variation of <4 % between the two light intensity tests led to model convergence. For example the low flux values at 4.87 W/m^2 of 4.85 L/m^2/h (data from Fig. 3) converged with the lower light intensity (3.08 W/m^2) values measured at 5.05 L/m^2/h, but did not converge with 'equivalent' values from flux measured at 4.70 L/m^2/h (data from Fig. 4). As only the results at measured flux of 4.85 L/m^2/h converged, the fitted $\beta/k_m.a_i$ parameters shown in Table 2 represented the low flux (5 L/m^2/h) condition. However further work has been identified from this finding, where accurate measurement of low fluxes to better understand the unique condition that has clearly appeared coinciding with the favourable phenol elimination at >90 %.

Table 2
Fitted model parameters from membrane L1 testing using Eqs. 8 to 12. $L = 15 \times 10^{-6}$ m, $\alpha = 1$, $\beta = 797{,}927$ 1/m.

Average measured flux, J (L/m^2/h)	Average superficial velocity, V_F (10^{-6} m/s)	Photocatalyst coating residence time, t_{res} (s)	$\beta/k_m.a_i$ (1/(m/s))	$k_m.a_i$ (1/s)
4.95	1.37	3.7	76,390	3.48
7.38	2.05	2.5	33,806	7.87
11.9	3.30	1.5	47,590	5.59

The model fitted $\beta/k_m.a_i$ for each same flux condition using different light intensities (I_0), and values were all in the same order of magnitude, ranging from 33,806 1/(m/s) for 7.4 L/m^2/h to 76,390 1/(m/s) for 5 L/m^2/h. Our values are higher than the literature reported value for the fixed bed PMR (FPMR) using methylene blue as the reactant, which obtained a $\beta/k_m.a_i$ value of 12,660 1/(m/s) [16] but still in the same order of magnitude. Differences to the previous study may be related to the different reactant methylene blue, but also the flow conditions as Duy Dũng et a 2017 [16] adopted significantly higher fluxes by at least two orders of magnitude, calculated to be in the range of 180–2500 L/m^2/h which is very high even for a practical ceramic membrane process with fluxed not exceeding 200 L/m^2/h [31,32]. In our system, the lowest value total mass transfer coefficient $k_m.a_i$ occurred for the lowest flux of 4.95 L/m^2/h as expected, but the next highest flux of 7.38 L/m^2/h gave the highest mass transfer coefficient as compared to the highest flux of 11.9 L/m^2/h. These two higher total mass transfer coefficient values may not be significantly different as compared to the lowest flux value.

Reaction rate modelling allows further comparison between fluxes

Table 3
Calculated reaction constants for membrane L1 calculated for specific fluxes and light intensity tests.

Flux J (L/m^2/h)	I_0 (W/m^2)	K_{res} (1/s)	k_{res} (10^{-6} m/s)	$K_{i,0}$ (1/s)	k_S (10^{-9} m/s)	k_S/I_0 (10^{-10} m^3/J)
5.05	3.08	0.386	5.46	1.80	2.80	9.10
7.41	3.08	0.340	5.04	1.46	2.58	8.38
11.8	3.08	0.344	5.17	1.56	2.65	8.61
4.85	4.87	0.522	7.83	2.85	4.02	8.25
7.36	4.87	0.507	7.61	2.43	3.90	8.01
11.9	4.87	0.511	7.68	2.47	3.94	8.09

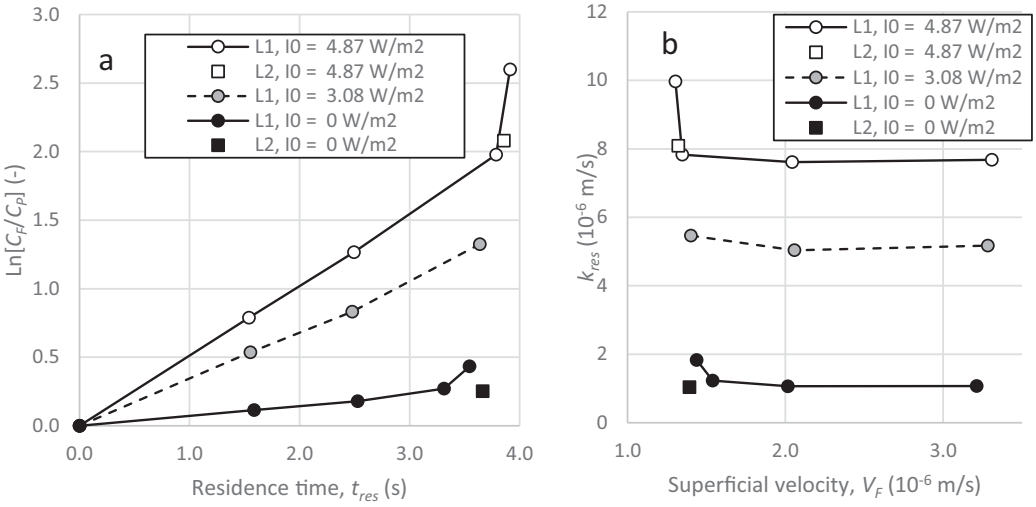

Fig. 10. Reaction kinetic graphs for all membrane tests (L1 and L2) carried out in light (both unattenuated and attenuated light intensities) and dark conditions, showing Ln(C_F/C_P) vs residence time t_{res} (a) and k_{res} as a function of superficial velocity (b).

and analyse reactor performance. The calculated values for K_{res} and k_{res} together with the model fitting determined value for $K_{i,0}$, are shown in Table 3. The lower total mass transfer coefficient $k_m.a_i$ at the flux of 4.95 L/m^2/h (Table 2) is consistent with the subsequently calculated combined reaction rate constant at the permeate surface of the photocatalyst $K_{i,0}$, for example showing a 23 % increase in reactivity from 7.4 to 4.9 L/m^2/h at I_0 = 4.87 W/m^2. These higher residence times and lower superficial velocities created favourable conditions for complete phenol conversion.

The surface reaction rate, k_S (m/s) is also included in Table 3 to better assist with comparisons of reaction rate to values reported by others using different immobilised catalyst properties as defined by Eq. 13 [16,33]:

$$k_S = \frac{K_{res}}{\rho_{cat} S_{cat}(1-\varepsilon)} \tag{13}$$

where ρ_{cat} is the density of the catalyst particle (kg/m^3) and S_{cat} is the specific surface area of catalyst particle (m^2/kg). A value of $\rho_{cat}S_{cat}$ = 1.97 × 10^8 m^2/m^3 was used by [16] in their fixed bed PMR and was used in the calculations here as the same P25 catalyst particles were used. Duy Dũng et al. 2017 [15] also further evaluated k_S by normalising to the light intensity I_0, i.e. k_S/I_0. The k_{res}, k_S and k_S/I_0 values in Table 3 can be compared to other studies in the literature, with the calculated values presented in Table 4.

The FPMR mode of operation testing with methylene blue at 15.3 W/m^2 UV intensity found k_{res} to be 43.5 × 10^{-6} m/s which is one order of magnitude higher than our value. However the prior reported k_S of 135 × 10^{-9} m/s is two orders of magnitude higher than current phenol test results. When normalised to the light energy k_S/I_0 the authors calculated a value of 7.2 × 10^{-9} m^3/J [16] is now back to one order of magnitude higher than the current modelled value. The differences could be due to the many assumptions used to calculate the value, such as the differing P25 bed properties and actual light energy reaching the catalyst coating. Assuming these are representative, there is, however, a similarity between the reaction kinetics for the systems and differences could relate to very different target organic molecules.

In looking to compare more closely on other tests with the same phenol molecule, no similar derivation of PMR reaction constants could be found in the literature (only constants derived for the given experimental reactor volume). The prior conventional immobilised PMR test showing phenol degradation through a P25 coated alumina membrane with light coming from above found 21 % phenol removal with the feed of 6 mg/L [17] were, however, closest to the current study test. Inputting their data into our model, and deriving their residence time for a 4 μm thick P25 coating of 0.14 s (assuming same porosity of 34 %), the k_{res}, k_S and k_S/I_0 values of 6.6 × 10^{-6} m/s, 12.3 × 10^{-9} m/s and 0.128 × 10^{-9} m^3/J respectively were calculated. When normalised to light intensity, I_0, the current values are within the same order of magnitude, with ours being 6.3-fold greater. This reaction rate is now comparable with our test result, with differences possibly due to of the use of a UV lamp (wavelength 315 nm to 400 nm) in the previous study, where the overall light energy used for photocatalysis may not have the same efficiency as a single wavelength LED (λ_{peak} = 365 nm) used in the current study, or that not all the light reached the photocatalyst surface in the previous study 4-tube reactor design, highlighting the benefit of the current study LT-PMR which resolves the light access issue. Further modelling can be found in the literature that has considered the interdependencies of the parameters and extended to a three-step mechanism explaining heterogeneous photocatalytic reactions, being generation of reactive charge carriers as Step 1, and either their recombination as Step 2 – or transfer to the target pollutant followed by its reaction as Step 3 [34]. Further work would be needed to develop a test regime for PMRs to extract all the relevant parameters, but may find more similarities in the reaction and mass transfer constants between setups, including batch vs PMRs.

There, however, appears to be alignment between the key reaction constants derived for PMRs when taking into account experimental differences, and of particular note is the similarity to the same molecule phenol in the light normalised value. The researchers in this work also noted that the reaction became less efficient when feed concentrations were increased (tested up to 94 mg/L phenol in the feed), concluding that PMRs for toxic contaminant removal are best designed for TrOC removal [17]. This appeared practically beneficial as toxic phenol in river water, drinking water, rainwater and ground water in certain locations can range from 0.075 to 10 μg/L, but also when upstream existing processes including biological treatment can already reduce them to low mg/L levels.

3.8. Utilisation of modelling parameters to understand confined reactions

In order to confirm the model parameters, and to predict the phenol concentrations as the solution transports through the confined pores of the LT-PMR catalyst coating, $C_{(z)}$ was graphed as a function of z (distance from catalyst surface facing the incoming light) according to [16] and adapted to account for the counter-current LT-PMR used in the current study where $C_0 = C_P$, as described by Eq. 14:

$$ln\frac{C_{(z)}}{C_P} = \frac{k_m a_i \varepsilon}{\alpha\beta V_F} ln\frac{k_m a_i + K_{i,0}}{k_m a_i + K_{i,0} e^{-\alpha\beta z}} \tag{14}$$

The results are presented in Fig. 11 for each of the modelled average fluxes using parameters from Tables 2 and 3 including light intensity as calculated using the relation that is part of widely used Lambert-Beer law that was used in deriving Eq. 15:

$$I_{(z)} = I_0 e^{-\beta z} \tag{15}$$

Fig. 11 shows the diminishing light intensity as it transmits through the photocatalyst coating from the permeate to the feed side. Meanwhile, the phenol concentration declines as it reacts within the photocatalyst coating as the solution moves from the feed (~10 mg/L phenol) to the permeate side (counter-current PMR). Higher fluxes lead to higher permeate phenol concentrations as described earlier. The profile of the phenol for the higher fluxes (~12 L/m^2/h and ~ 7.4 L/m^2/h) shows an accelerating decline as the solution approaches the light source, corresponding to higher light intensities and therefore faster reaction rates. The profile evolves for the lower flux (~5 L/m^2/h) to a more linear appearance in the middle of the coating (z/L = 0.5), showing a greater

Table 4
Comparison of reaction constants from this work with literature on PMRs for the intrinsic reaction rate constant per unit of cross section area of the catalyst layer, k_{res}, surface reaction rate constant of the catalyst layer, k_S, and light intensity normalised surface reaction rate constant, k_S/I_0.

PMR type	Feed solution	Light intensity (W/m^2)	k_{res} (10^{-6} m/s)	k_S (10^{-9} m/s)	k_S/I_0 (10^{-9} m^3/J)	Reference
Fixed bed PMR (FPMR)	3.2 mg/L methylene blue	15.3 (UVA lamp)	43.5*	135	7.2	[16]
Conventional immobilised PMR	6 mg/L phenol	100 (UV lamp)	6.64^	12.3	0.128	[17]
Light transmitting immobilised PMR (LT-PMR)	10 mg/L phenol in 20 mg/L NaCl	4.87 (UV LED @365 nm)	7.71	3.95	0.812	This work

*k_{res} calculated by Eq. 18 that appeared in reference [16].
^ k_{res} calculated from phenol feed and permeate concentration data presented at flux of 34.5 L/m^2/h and membrane thickness of 4 μm reported in reference [17] by Eqs. 6, 7 and 9 and assumed porosity of 34 %.

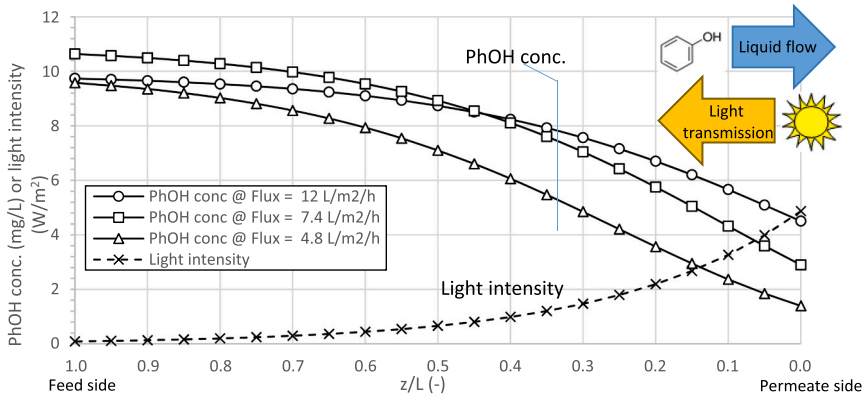

Fig. 11. Counter-current LT-PMR model calculation of phenol (PhOH) concentration ($C_{(z)}$) and light intensity ($I_{(Z)}$) as a function of the normalised length (z/L) through the photocatalyst coating at the three tested fluxes. $I_0 = 4.87$ W/m^2. Feed solution of ~10 mg/L phenol enters on the left ($z/L = 1.0$) and permeates through the coating while reacting phenol, leaving as discharged permeate at the same location that light enters the PMR ($z/L = 0.0$).

phenol reduction at greater distance from the light source. This correlates with the low concentrations of degradation by-products shown in the HPLC analysis. It may also correlate to the unique finding in the model for this flux for high $\beta/\ k_m.a_i$ fitted values relative to the other two fluxes (Table 2). This ultimately leads to a uniquely lower total mass transfer coefficient $k_m.a_i$ and higher combined reaction rate constant at the permeate side $K_{i,0}$, indicating the mass transfer and photocatalyst surface conditions were more favourable for phenol mineralisation.

4. Conclusions

PMRs are a promising AOP for destruction of TrOCs needed for realising sustainable water supply from abundant contaminated sources such as wastewater and stormwater. With advancements in PMRs, this form of AOP appears to be progressing into practical realisation, particularly since dead-end modes and light transmitting substrates have been explored by researchers. This study tested toxic phenol degradation in a novel LT-PMR in dead-end mode with no recirculation in feed or permeate and found up to 93 % phenol degradation with the majority occurring by mineralisation as measured by TOC and HPLC. This was achieved at fluxes around 5 L/m^2/h. Modelling of the LT-PMR as a counter-current system (light direction opposite to flux direction) found comparable reaction constants and mass transfer coefficients to those found in prior PMR research literature for the same target molecule, and that higher reaction rates occurred as phenol concentration in the photocatalyst coating decreased, indicating the value of the LT-PMR for residual pollutant destruction. More work is needed on the low energy and highly practical dead-end mode PMRs in order to improve model accuracy, as well as studies on improved light transmission and photocatalytic materials and exploration on more contaminants in real water matrices.

CRediT authorship contribution statement

Peter Sanciolo: Writing – review & editing, Writing – original draft, Methodology, Investigation, Formal analysis, Data curation, Conceptualization. **Kana Moriguchi:** Writing – review & editing, Methodology, Investigation, Formal analysis, Data curation. **Noel Dow:** Writing – review & editing, Methodology, Formal analysis, Data curation. **Fotios Sidiroglou:** Writing – review & editing. **Tomohisa Yoshioka:** Writing – review & editing, Supervision, Methodology, Investigation, Formal analysis, Data curation, Conceptualization. **Keizo Nakagawa:** Writing – review & editing, Supervision, Methodology, Investigation, Formal analysis, Data curation, Conceptualization. **Mikel Duke:** Writing – review & editing, Writing – original draft, Supervision, Resources, Project administration, Methodology, Investigation, Formal analysis, Data curation, Conceptualization.

Declaration of competing interest

The authors declare that they have no known competing financial interests or personal relationships that could have appeared to influence the work reported in this paper.

Data availability

Data will be made available on request.

Acknowledgements

The authors would like to acknowledge the internal financial support from Victoria University for this study. The authors would also like to thank Lavern T. Nyamutswa for the preparation of the P25 coated membranes used in this work.

References

[1] Y. Luo, W. Guo, H.H. Ngo, L.D. Nghiem, F.I. Hai, J. Zhang, S. Liang, X.C. Wang, A review on the occurrence of micropollutants in the aquatic environment and their fate and removal during wastewater treatment, Sci. Total Environ. 473-474 (2014) 619–641.
[2] N. Konradt, J.G. Kuhlen, H.-P. Rohns, B. Schmitt, U. Fischer, T. Binder, V. Schumacher, C. Wagner, S. Kamphausen, U. Müller, F. Sacher, P. Janknecht, R. Hobby, I.M.A. ElSherbiny, S. Panglisch, Removal of trace organic contaminants by parallel operation of reverse osmosis and granular activated carbon for drinking water treatment, Membranes 11 (1) (2021) 33.
[3] P. Mahbub, M. Duke, Scalability of advanced oxidation processes (AOPs) in industrial applications: a review, J. Environ. Manag. 345 (2023) 118861.
[4] H. Wang, X. Li, X. Zhao, C. Li, X. Song, P. Zhang, P. Huo, X. Li, A review on heterogeneous photocatalysis for environmental remediation: from semiconductors to modification strategies, Chin. J. Catal. 43 (2) (2022) 178–214.
[5] D.R. Eddy, S.N. Ishmah, M.D. Permana, M.L. Firdaus, I. Rahayu, Y.A. El-Badry, E. E. Hussein, Z.M. El-Bahy, Photocatalytic phenol degradation by silica-modified titanium dioxide, Appl. Sci. 11 (19) (2021) 9033.
[6] D. Vione, C. Minero, V. Maurino, M.E. Carlotti, T. Picatonotto, E. Pelizzetti, Degradation of phenol and benzoic acid in the presence of a TiO2-based heterogeneous photocatalyst, Appl. Catal. B Environ. 58 (1) (2005) 79–88.
[7] C.-H. Chiou, C.-Y. Wu, R.-S. Juang, Influence of operating parameters on photocatalytic degradation of phenol in UV/TiO2 process, Chem. Eng. J. 139 (2) (2008) 322–329.
[8] M.N. Subramaniam, P.S. Goh, D. Kanakaraju, J.W. Lim, W.J. Lau, A.F. Ismail, Photocatalytic membranes: a new perspective for persistent organic pollutants removal, Environ. Sci. Pollut. Res. 29 (9) (2022) 12506–12530.
[9] N. Nasrollahi, L. Ghalamchi, V. Vatanpour, A. Khataee, Photocatalytic-membrane technology: a critical review for membrane fouling mitigation, J. Ind. Eng. Chem. 93 (2021) 101–116.
[10] H. Zhang, Y. Wan, J. Luo, S.B. Darling, Drawing on membrane photocatalysis for fouling mitigation, ACS Appl. Mater. Interfaces 13 (13) (2021) 14844–14865.
[11] J. Zhang, H. Wu, L. Shi, Z. Wu, S. Zhang, S. Wang, H. Sun, Photocatalysis coupling with membrane technology for sustainable and continuous purification of wastewater, Sep. Purif. Technol. 329 (2024) 125225.

[12] C.H. Kirk, P. Wang, C.Y.D. Chong, Q. Zhao, J. Sun, J. Wang, TiO2 photocatalytic ceramic membranes for water and wastewater treatment: technical readiness and pathway ahead, J. Mater. Sci. Technol. 183 (2024) 152–164.
[13] M. Schwarze, S. Borchardt, M.L. Frisch, J. Collis, C. Walter, P.W. Menezes, P. Strasser, M. Driess, M. Tasbihi, Degradation of phenol via an advanced oxidation process (AOP) with immobilized commercial titanium dioxide (TiO2) photocatalysts, Nanomaterials 13 (7) (2023) 1249.
[14] M. Binazadeh, J. Rasouli, S. Sabbaghi, S.M. Mousavi, S.A. Hashemi, C.W. Lai, An overview of photocatalytic membrane degradation development, Materials 16 (9) (2023) 3526.
[15] S.A. Heredia Deba, B.A. Wols, D.R. Yntema, R.G.H. Lammertink, Transport and surface reaction model of a photocatalytic membrane during the radical filtration of methylene blue, Chem. Eng. Sci. 254 (2022) 117617.
[16] P. Duy Dũng, F. Babick, M.T. Nguyen, B. Wessely, M. Stintz, Modelling the influence of mass transfer on fixed-bed photocatalytic membrane reactors, Chem. Eng. Sci. 173 (2017) 242–252.
[17] S. Deepracha, L. Atfane, A. Ayral, M. Ogawa, Simple and efficient method for functionalizing photocatalytic ceramic membranes and assessment of its applicability for wastewater treatment in up-scalable membrane reactors, Sep. Purif. Technol. 262 (2021) 118307.
[18] L.T. Nyamutswa, B. Hanson, D. Navaratna, S.F. Collins, K.G. Linden, M.C. Duke, Sunlight-transmitting photocatalytic membrane for reduced maintenance water treatment, ACS ES&T Water 1 (9) (2021) 2001–2011.
[19] L.T. Nyamutswa, B. Zhu, S.F. Collins, D. Navaratna, M.C. Duke, Light conducting photocatalytic membrane for chemical-free fouling control in water treatment, J. Membr. Sci. 604 (2020) 118018.
[20] L.T. Nyamutswa, B. Zhu, D. Navaratna, S. Collins, M.C. Duke, Proof of concept for light conducting membrane substrate for UV-activated photocatalysis as an alternative to chemical cleaning, Membranes 8 (4) (2018) 122.
[21] L.T. Nyamutswa, S.F. Collins, D. Navaratna, M.C. Duke, Concept demonstration and future developments of sunlight transmitting nanophotocatalyst-coated substrates for sustainable low pressure water filtration, in: Y. Cohen (Ed.), The World Scientific Reference of Water Science, World Scientific, 2021, pp. 419–457.
[22] B. Wang, L. Shen, J. Xu, L. Fei, B. Li, H. Lin, C. Chen, Spiropyran molecular aggregates implanted photo-responsive graphene oxide membrane with self-cleaning ability for enhanced water purification, J. Membr. Sci. 702 (2024) 122744.
[23] L.G.C. Villegas, N. Mashhadi, M. Chen, D. Mukherjee, K.E. Taylor, N. Biswas, A short review of techniques for phenol removal from wastewater, Curr. Pollut. Rep. 2 (3) (2016) 157–167.
[24] R.K. Herz, Intrinsic kinetics of first-order reactions in photocatalytic membranes and layers, Chem. Eng. J. 99 (3) (2004) 237–245.
[25] D. Chen, F. Li, A.K. Ray, Effect of mass transfer and catalyst layer thickness on photocatalytic reaction, AICHE J. 46 (5) (2000) 1034–1045.
[26] D.F. Ollis, Kinetic disguises in heterogeneous photocatalysis, Top. Catal. 35 (3) (2005) 217–223.
[27] S. Imoto, K. Nakagawa, C. Hu, T. Yoshioka, T. Shintani, A. Matsuoka, E. Kamio, T. Tachikawa, S.C.E. Tsang, H. Matsuyama, HNb3O8/g-C3N4 nanosheet composite membranes with two-dimensional heterostructured nanochannels achieve enhanced water permeance and photocatalytic activity, Chem. Eng. J. 442 (2022) 136254.
[28] Y. Tao, Z.L. Cheng, K.E. Ting, X.J. Yin, Photocatalytic degradation of phenol using a nanocatalyst: the mechanism and kinetics, J. Catal. 2013 (2013) 364275.
[29] S. Yohi, C.-M. Wu, R.T. Koodali, A kinetic study of photocatalytic degradation of phenol over titania–silica mixed oxide materials under UV illumination, Catalysts 12 (2) (2022) 193.
[30] A. Sobczyński, Ł. Duczmal, W. Zmudziński, Phenol destruction by photocatalysis on TiO2: an attempt to solve the reaction mechanism, J. Mol. Catal. A Chem. 213 (2) (2004) 225–230.
[31] N. Dow, D. Murphy, J. Clement, M. Duke, Outcomes of the Australian ozone/ceramic membrane trial on secondary effluent, AWA Water 40 (6) (2013) 45–51.
[32] N. Dow, J. Roehr, D. Murphy, L. Solomon, J. Mieog, J. Blackbeard, S. Gray, N. Milne, B. Zhu, A. Gooding, J. Currie, G. Roeszler, J. Clement, M. Duke, Fouling mechanisms and reduced chemical potential of ceramic membranes combined with ozone, Water Practice & Technology 10 (4) (2015) 806–813.
[33] A. Visan, D. Rafieian, W. Ogieglo, R.G.H. Lammertink, Modeling intrinsic kinetics in immobilized photocatalytic microreactors, Appl. Catal. B Environ. 150-151 (2014) 93–100.
[34] J.Z. Bloh, A holistic approach to model the kinetics of photocatalytic reactions, Frontiers in Chemistry (2019) 7.